FUDMA Journal of Sciences (FJS)
ISSN online: 2616-1370
ISSN print: 2645 - 2944
Vol. 4 No. 1, March, 2020, pp 190 – 199

THERMALLY STABLE DYSPROSIUM DOPED ZINC-SODIUM-TELLURITE GLASSES: ABSORPTION AND EMISSION PROPERTIES ENHANCEMENT

[*1, 2]Badamasi, S., [3,4]Tanko, Y. A., [5,6]Yamusa, Y. A., [7]Garba, N. N. & [8]Najamuddeen Musa, M.

[1,3,5]Department of Physics, Faculty of Science, Universiti Teknologi Malaysia, 81310 Skudai, Johor, Malaysia.
[2]Technical Department, N.B.T.I.-Technology Incubation Centre, Kano, TIC Complex Farm Centre, Kano State, Nigeria.
[4]Department of Physics, Kaduna State University (KASU), Kaduna, Nigeria.
[6]Centre for Energy Research and Training, Ahmadu Bello University, Zaria, Nigeria.
[7]Department of Physics, Ahmadu Bello University, Zaria, Nigeria.
[8]Nigerian Nuclear Regulatory Authority, North-West Zonal Office, Kano, Nigeria.

[*]Corresponding Authors' email: suleimanbadamasi19@gmail.com

ABSTRACT

Tellurium dioxide among the numerous glass formers have been of interest to researchers due to its promising characteristics. Consequently, absorption and emission are among the most paramount features of glasses applicable in lasers and other optical devices, but there are not much report on absorption and emission properties of Zinc-Sodium-Tellurite Dysprosium doped glasses. Series of dysprosium (Dy^{3+}) ions doped zinc-sodium-tellurite glass having composition (65-x)TeO_2-25ZnO-10Na_2O-xDy_2O_3 ($0 \leq x \leq 2.5$ mol%) were prepared using melt-quenching method. Transparent and thermally stable glass samples were characterized via UV-Vis-NIR absorption, photoluminescence (PL), and Fourier transform infrared (FTIR) spectroscopy. Density and molar volume of prepared glass system were found to be in the range of 5.334-5.366 gm^{-3} and 24.425-25.273 cm^3mol^{-1}, respectively. FTIR spectra exhibited various bonding vibrations corresponding to glass network structures and units. UV-Vis-NIR spectra revealed seven absorption peaks centred at 450, 752, 801, 901, 1095, 1281, and 1687 nm which were assigned to the transitions from the ground state to the excited levels such as$^6H_{15/2} \rightarrow {}^4F_{9/2}$, $^6H_{15/2} \rightarrow {}^6F_{3/2}$, $^6H_{15/2} \rightarrow {}^6F_{5/2}$, $^6H_{15/2} \rightarrow {}^6F_{7/2}$, $^6H_{15/2} \rightarrow {}^6H_{7/2}$, $^6H_{15/2} \rightarrow {}^6F_{11/2}$, and $^6H_{15/2} \rightarrow {}^6H_{11/2}$ of Dysprosium Dy^{3+} ions, respectively. Room temperature PL spectra displayed three significant peaks centred at 497, 588, and 675 nm, which were allocated to the transitions from $^4F_{9/2}$ excited state to the $^6H_{11/2}$, $^6H_{13/2}$, and $^6H_{15/2}$ states, respectively. Present optimized glass composition may be potential for the development of solid state lasers and photonic devices.

Keywords: Tellurite glass, Melt-quenching method, Absorption spectra, Emission spectra and Differential Thermal Analyser.

INTRODUCTION

In the past decades, the optical properties of rare-earth ions (REIs) doped binary and ternary glasses have been comprehensively studied owing to their several applications in optical switching, solid state lasers, optical data storage, display monitor, sensors etc. (Agarwal et al, 2009). Amongst all glass systems, tellurite-based glasses are attractive due to their excellent attributes including low phonon energy, high refractive index, and low melting point, besides good chemical and thermal stability (Wang, *et al*, 1994; El-Mallawany, 2002; Kumar, *et al*, 2006; Badamasi, 2017). When heavy metal oxides such as Pb, Mg, and Zn are being introduced into a tellurite glass, it reveals reasonable modifications in the physical and optical properties of the host. Thus, such glass systems are favourable for fabricating luminescent and nonlinear optical devices provided their optical gain is enhanced.

The optical properties of Dysprosium (Dy^{3+}) ions doped glasses are distinct because such trivalent ions reveal broad and intense emission bands corresponding to the optical transitions of $^4F_{9/2} \rightarrow {}^6H_J$ (J = 15/2, 13/2, 11/2) upon the selection of an appropriate host matrix. Dy^{3+} is one of the essential rare-earth phosphors for manufacturing varieties of light-emitting materials. The luminescence spectrum of Dy^{3+} is comprised of two strong bands including $^4F_{9/2}$-$^6H_{15/2}$ (blue) and $^4F_{9/2}$-$^6H_{13/2}$ (yellow) in the visible region and a red luminescence band arises from $^4F_{9/2}$-$^6H_{11/2}$ transition. Earlier, several researchers examined the luminescent properties of Dy^{3+} ions incorporated in various amorphous and crystalline compounds (Lakshminarayana & Buddhudu, 2006; Abdul Azeem, *et al*, 2008; Praveena, R., & Jayasankar, 2008; Pisarska, 2009; Babu, *et al*., 2010; Pisarska, *et al*, 2010; Kesavulu & Jayasankar, 2011; Madhukar Reddy, *et al*, 2011; Maheshvaran & Marimuthu, 2011; Saleem, *et al*, 2011; Kumar, *et al*, 2012; Pisarski, *et al*, 2012; Reddy, *et al*., 2012; Krishnaiah, *et al*, 2013; Linganna, *et al*, 2013; Sreedhar, *et al*,

2013; Badamasi, 2017). Furthermore, the intensities of the emission bands of Dy^{3+} ion in a particular media is decided by its concentration as well as the host glass composition (Tanko, *et al*, 2016). In attaining superior spectroscopic properties, the selection of overall composition is prerequisite for device applications.

This paper reports the systematic characterizations and spectral analysis of Dy^{3+} ions doped zinc-sodium-tellurite glasses synthesized via melt quenching method. Dy^{3+} ion concentration dependent variation in the density, molar volume, refractive index, and optical band gaps of the prepared glass system are evaluated. The influence of Dy^{3+} ions contents on the absorption and emission properties of the prepared glasses are examined and discussed.

MATERIALS AND METHODS

Six glass samples with chemical composition of (65-x)TeO_2–25ZnO–10Na_2O–xDy_2O_3 (x= 0.0, 0., 0.8, 1.2, 1.6, and 2.5 mol%) were prepared using conventional melt-quenching method. Analytical grade (99.99% purity, Sigma Aldrich) powders of TeO_2, ZnO, Na_2O, and Dy_2O_3 (TZND0.0, TZND0.4, TZND0.8, TZND1.2, TZND1.6 and TZND2.5) were chosen for sample preparation. The details of the glass compositions and their codes are summarized in Table 1.

Mixed glass constituents of about 15 g batches were well mixed in a platinum crucible before being placed into the furnace at 900 ℃ for about 10 minutes to have complete melting. Upon achieving the desired viscosity, the melt was casted into a preheated steel mould and annealed at 250 ℃ for 3 h to reduce the thermal stress that may cause further embrittlement. Then, the samples were cooled down to room temperature for almost 24 hours before being cut and polished for optical measurements.

To verify the amorphous nature of the glasses, X-ray Diffraction (XRD) analysis was carried out on Siemens Diffractometer D5000 using Cu Kα radiations (k = 1.54 Å) at 40 kV and 100 mA, with scanning angle 2θ ranges between 10° and 80°. Room temperature absorption spectra in the range of 400–1600 nm were recorded using a Shimadzu UV-3101PC scanning spectrophotometer (Kyoto, Japan). Photoluminescence (PL) emission measurements were performed using a Perkin Elmer LS-55 luminescence spectrometer in which a pulsed Xenon lamp was used for excitation. The emitted light was dispersed by Monk–Gillieson monochromator and detected with the standard photomultiplier tube.

Archimedes method was used to determine the glass density (ρ, in g.cm^{-3}) with toluene as an immersion liquid and expressed as:

$$\rho = \frac{W_a}{W_a - W_l}\left(\rho_l - \rho_a\right) + \rho_a \qquad (1)$$

where W_a and W_l are the weight of glass in air and in liquid, respectively. ρ_a and ρ_l are the density of air (0.001 g.cm^{-3}) and toluene (0.8669 g.cm^{-3}), respectively. The molar volume (V_m) in terms of molar mass (M) yields (Badamasi & Tanko, 2018; Yamusa, *et al*, 2018):

$$V_m = \frac{M}{\rho} \qquad (2)$$

The UV-Vis absorption edge data was used to determine the optical band gap (E_g), where Davis Mott equation and Tauc method were utilized (Badamasi, 2017; Badamasi & Tanko, 2018). The absorption coefficient α is estimated via:

$$\alpha(\upsilon) = \frac{const}{h\upsilon}\left(h\upsilon - E_g\right)^r \qquad (3)$$

where $h\nu$ is the incident photon energy, $\nu$is the frequency of incident radiation, r is the optical transition index (r = ½ for allowed direct transition and r = 2 for allowed indirect transition), E_g is the optical band gap energy, and *const* is a band tailing parameter. Value of band gap energy is acquired by extrapolating the linear part of the graph of $(\alpha h\nu)^{1/2}$ against $h\nu$ to the point where$(\alpha h\nu)^{1/2}$ = 0. The refractive index of the glass is calculated following Lorentz-Lorenz relation:

$$R_m = \frac{n-1}{n+2}V_m \qquad (4)$$

where R_m is molar refractivity, n is the refractive index and V_m as earlier defined. Table 2 enlists the values of density, molar volume, band gap energy and refractive index of all prepared glass samples.

Thermal properties of the glasses were checked using differential thermal analyzer of Perkin Elmer DTA-7 model. A sample of 11mg in powder form was heated at 10℃/min. The machine operated under a dry nitrogen atmosphere with flow rate of about 200 ml/min. The Hruby parameter H is used to estimate the stability of the prepared glasses from the relation

$$H_g = \frac{T_c - T_g}{T_m - T_c} \qquad (5)$$

Table. 1. Nominal composition of prepared glass samples with codes

Sample codes	Glass composition			
	TeO_2 (mol%)	ZnO (mol%)	Na_2O (mol%)	Dy_2O_3 (mol%)
TZND0.0	65.0	25.0	10.0	0.0
TZND0.4	64.6	25.0	10.0	0.4
TZND0.8	64.2	25.0	10.0	0.8
TZND1.2	63.8	25.0	10.0	1.2
TZND1.6	63.4	25.0	10.0	1.6
TZND2.5	62.5	25.0	10.0	2.5

Table. 2. Some physical and optical properties of the prepared samples.

Sample codes	Physical parameters			
	P ($g.cm^{-3}$)	V_m ($cm^3.mol^{-1}$)	E_g (eV)	*n*
TZND0.0	5.334	24.425	2.67	2.492
TZND0.4	5.342	24.548	2.67	2.492
TZND0.8	5.352	24.661	2.66	2.495
TZND1.2	5.358	24.793	2.64	2.501
TZND1.6	5.361	24.938	2.46	2.560
TZND2.5	5.366	25.273	2.30	2.617

RESULTS AND DISCUSSIONS

Figure 1 shows the typical XRD pattern of the prepared glass samples. The complete absence of any sharp crystalline peaks and the presence of a broad halo clearly indicated the true amorphous nature of the prepared glasses (Zarifah, *et al*, 2010; Badamasi, 2017).

Figure 2 displays the room temperature UV–Vis–NIR absorption spectra for the prepared samples. The absorption spectra divulge seven significant bands centred at 450, 752, 801, 901, 800, 1095, 1281 and 1687 nm. Appearance of these peaks are assigned to the absorptions from the Dy^{3+} ions ground state of $^6H_{15/2}$ to the excited states of $^4F_{9/2}$, $^6F_{3/2}$, $^6F_{5/2}$, $^6F_{7/2}$, $^6H_{7/2}$, $^6F_{11/2}$ and $^6H_{11/2}$, respectively as agreed with other findings (Damak *et al*, 2014; Badamasi, 2017). From Table2, it is clearly seen that both the density and molar volume increases with increasing concentration of dysprosium ions. The increase in density with increasing dopant content is as a result in the close arrangement of atoms and increase in bond between the molecules. Therefore, the observed changes in the glass density may reflect the differences in the glass composition and in turn the network structure. The observed decrease in the value of E_g (Table 2) from 2.67 to 2.30 eV with increasing of Dy^{3+} ions content is attributed to the generation of higher nucleation sites for the crystallization and formation of oxygen bridging networks which leads to the minimum defects in the host matrix of the prepared glasses. The achieved value of E_g is comparable to the earlier reported work on tellurite-based glass systems (Damak, *et al*, 2014; Badamasi & Tanko, 2018). It was observed that with increasing dysprosium ions content in the glass host the refractive index also increases from 2.492 to 2.617. Since, the interaction between light and the electron clouds of the constituent atoms and ions of the glass determined the refractive index of a glass, increasing in both electron density and polarizability of the ions increase the refractive index. Furthermore, increase in refractive index could be due to increase in the structural disorder and increase in the internal stress of the glass materials.

Figure 3 illustrates the room temperature luminescence spectra under 410 nm laser excitations. The observed three prominent emission bands centred at 497 nm, 588 nm and 675 nm are assigned to the transitions from the excited states of $^4F_{9/2}$ to $^6H_{11/2}$ magnetic dipole obeying $\Delta J = 0, \pm 1$ and $0 \leftrightarrow 0$ selection rule, $^6H_{13/2}$ which is an electric dipole and hypersensitive obeying the $|\Delta L| \leq 2$, $|\Delta J| \leq 2$, selection rule, to the ground state $^6H_{15/2}$ of Dy^{3+} ions, and lastly $^6H_{15/2}$ in red region is electric dipole and relatively weaker than the first two respectively. The obtained emission peaks of the glass system confirmed the presence of trivalent Dy^{3+} ions in the host network (Damak *et al*, 2014; Badamasi, 2017).

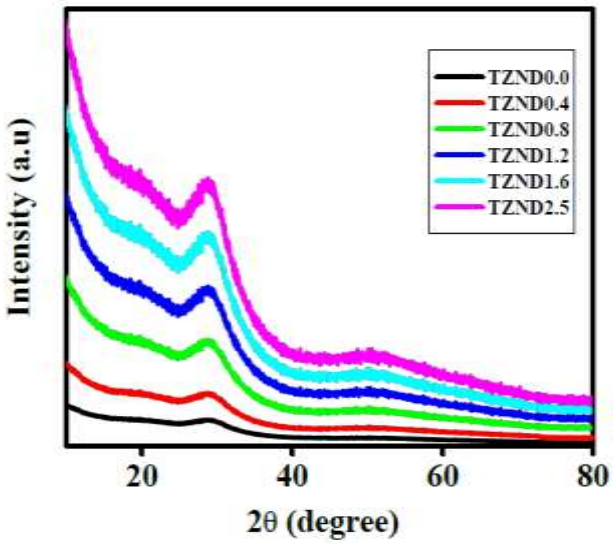

Fig. 1. XRD pattern of all prepared glass samples

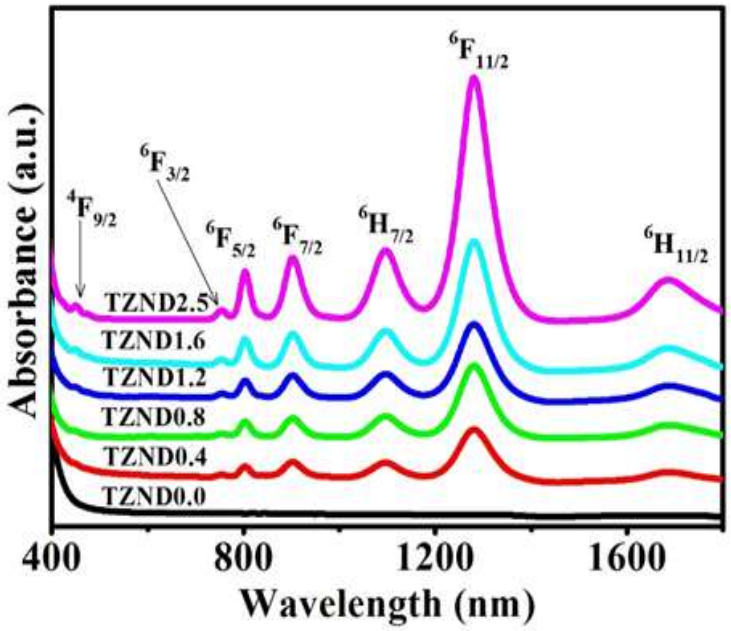

Fig. 2. UV-Vis absorption spectra of all prepared glass samples.

Figure 4 depicts the Dy^{3+} ions concentration dependent integrated luminescence intensity enhancement factor (η_{max}) of various peaks for all glass system. Table 3 enlists the values of η_{max} for different glass composition, where intensities of all the bands are significantly enhanced. The glass with 0.8 mol% of Dy^{3+} exhibited the highest intensity in the entire spectral range with an enhancement factor of 1.54 (for yellow) and 1.63 (for blue) bands. The maximum amplification for the red band (1.46) occurred for TZND1.2 sample. The photoluminescence intensity depends on the absorption, radiative emissions and non- radiative energy dissipation rates in the host material system. The photoluminescence is caused by suppression of photoluminescence blinking and electric field enhancement due to localized Plasmon excitation. Furthermore, these enhancements are influenced by the local environment around Dy^{3+} ions in the host matrix. It is found that the luminescent strength attenuated with further addition of at 1.6 mol% and 2.5 mol% dysprosium ion concentration, this occurred due to concentration quenching which happens because of the energy transfer between Dy^{3+} ions and Dy^{3+}.

The aforementioned three visible emissions, together with the excitation wavelength of 410 nm, are illustrated in the energy level diagram in Figure 5.The energy diagram describes the excitations, emissions and other processes such as radiative and non-radiative energy transfer. First, the Dy^{3+} ions are excited by 410 nm radiation from the ground state $^6H_{15/2}$ to most excited level $^4F_{7/2}$ which then decay non-radiatively to $^4I_{15/2}$ and $^4F_{9/2}$ states before making $^4F_{9/2}\rightarrow{}^6H_{15/2}$, $^4F_{9/2}\rightarrow{}^6H_{13/2}$ and $^4F_{9/2}\rightarrow{}^6H_{11/2}$ downward transition radiatively giving blue, yellow and red emissions, respectively (Damak, *et al*, 2014; Badamasi, 2017).

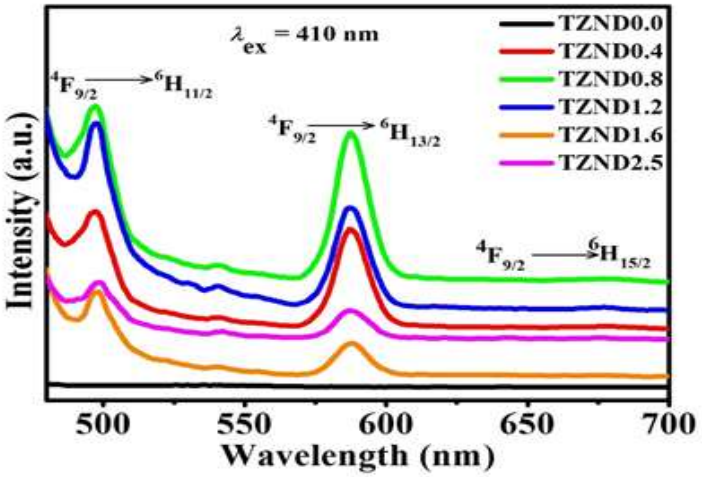

Fig. 3. Luminescence spectra of all glass samples under 410 nm excitations.

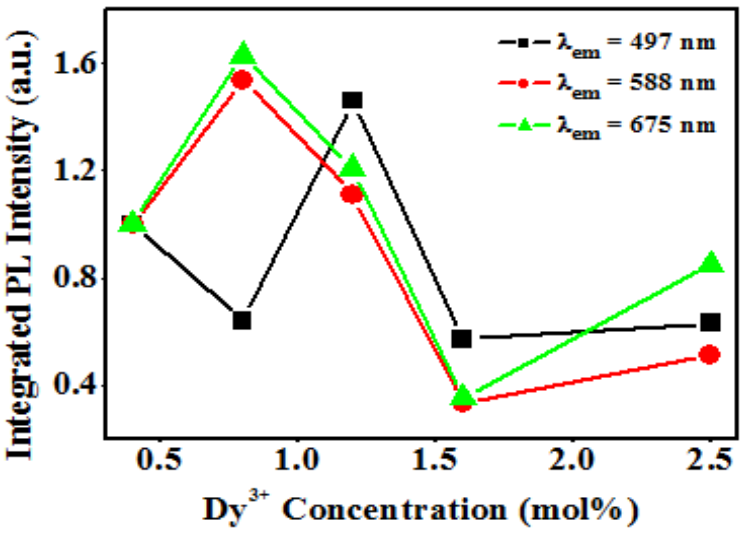

Fig. 4. Dy^{3+} ions concentration dependent integrated PL intensity enhancement factor.

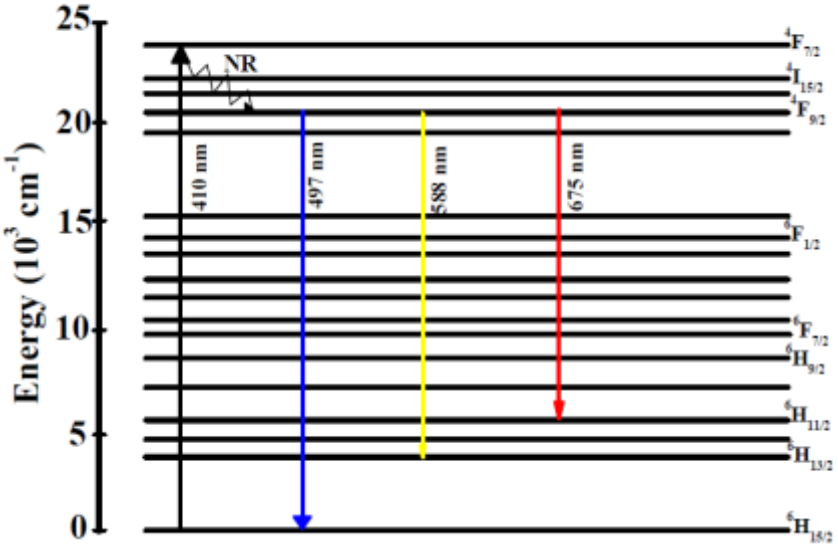

Fig. 5. Energy level diagram of Dy^{3+} ion in zinc tellurite glass.

Table. 3. The maximum PL intensity enhancement factor for different Dy_2O_3 content.

Sample code	Dy_2O_3 (mol%)	η_{max}(497:588:675)
TZND0.4	0.4	1:1:1
TZND0.8	0.8	0.64:1.54:1.63
TZND1.2	1.2	1.46:1.11:1.21
TZND1.6	1.6	0.57:0.33:0.35
TZND2.5	2.5	0.63:0.51:0.85

Figure 6 illustrates the FTIR spectra of all the prepared glass sample. The presence of bands in the wavenumber region of 448−461 cm^{-1} are assigned to ZnO bond vibration (El-Zaidia, *et al*, 1985; Badamasi, 2017). The bands in the range of 488−490 cm^{-1} are allocated to the Zn-O tetrahedral bond vibration. The absorption band centred at 640 cm^{-1} is the characteristics of pure TeO_2 units (El-Zaidia, *et al*, 1985). The presence of two bands around 615 and 660 cm^{-1} are allocated to the TeO_4 and TeO_3 structural units, respectively (Gowda, *et al*., 2007; Rada, *et al*, 2011; Badamasi, 2017). The broadening of these bands in relation to the crystalline TeO_2 is apparent as a result to wide distribution of bond angles and lengths in the amorphous matrix (Rada, *et al*, 2011). Moreover, the conversion of TeO_4 tbp units to TeO_3 tbp units causes a reduction in the number of TeO_4 groups. The vibrations of adsorbed water molecule in the glass give rise to bands at around 1625−1661 cm^{-1}. The bands in the range of 2925−2944 cm^{-1} are related to the stretching vibrations of hydrogen bond (Rada, *et al*, 2011). The stretching vibration of OH caused strong absorption in the range of 3445−3482 cm^{-1} (Maheshvaran & Marimuthu, *et al*, 2011; Badamasi, 2017).

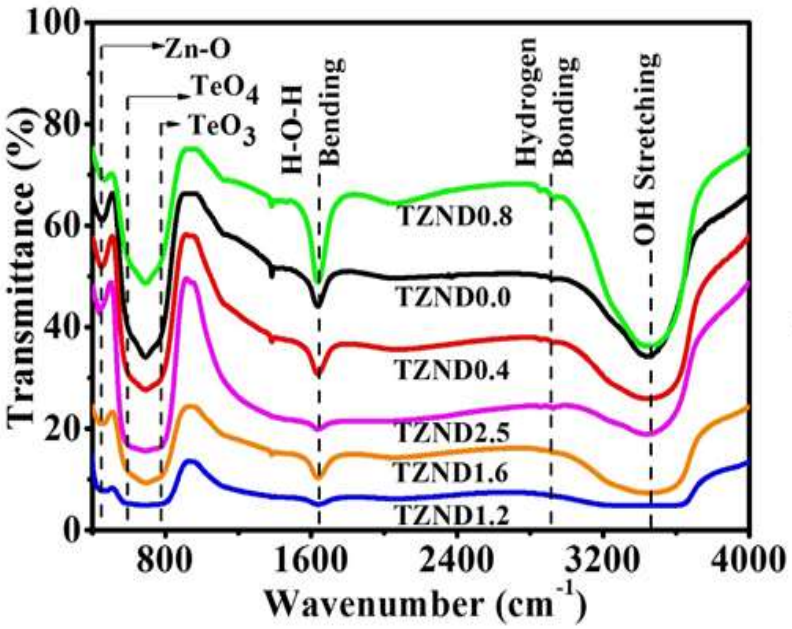

Fig. 6. FTIR spectra of the prepared glass sample.

Table 4 summarized the FTIR band position and their assignment. The band around 448-468 cm^{-1} is assigned to vibrations of Zn-O bond in ZnO_4 units. Conversely, the bands at 560-615 cm^{-1}, 772-817 cm^{-1}, 1625-1661 cm^{-1}, 2925-2944 cm^{-1} and 3445-3482 cm^{-1} are assigned to the bending vibrations of Te-O linkage in TeO_4 units, bending vibrations of Te-O linkage in TeO_3 units, vibrations of water molecule, hydrogen bond vibration and stretching of OH group, respectively.

Table. 4. FTIR band positions and band assignments of all glass sample

Band positions (cm^{-1}) of various simple						Bands assignment
TZND0.0	TZND0.4	TZND0.8	TZND1.2	TZND1.6	TZND2.5	
448	453	462	468	481	468	Vibrations of Zn-O bond (ZnO_4)
615	590	599	591	604	560	Bending vibrations Te-O in TeO_4 units
772	785	795	811	811	817	Bending vibrations of Te-O in TeO_3 units
1625	1636	1646	1654	1655	1661	Vibrations of water molecule
2925	2928	2936	2937	2938	2944	Hydrogen bonding
3445	3455	3464	3473	3476	3482	Stretching of OH group

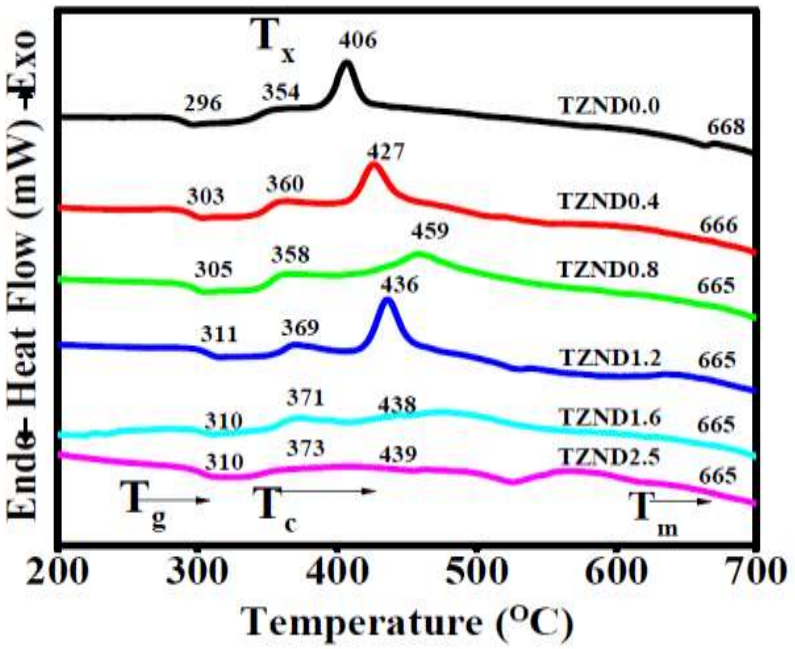

Fig. 7.DTA curves of Dy^{3+}doped Zinc Sodium Telluride glasses

The results of DTA measurements are shown in Fig.7**.** The endothermic peak corresponds to the melting temperature (T_m) at 665-668 °*C*, the exothermic peak corresponds to the crystallization temperature (T_c) at 406-459 °*C* and the tiny peak corresponds to the glass transition temperature (T_g) at 296-311°*C*.Glass transition temperature increase from 0.0 mol% up to 1.2 mol% and then decrease at 1.6 mol% and 2.5 mol% with the increase of Dy^{3+}concentarion. These results show that the addition of Dy_2O_3 causes an increase in the rigidity of the glass network formed by TeO_3tp units and the increase of non-bringing oxygen atoms in these glasses. The magnitude (T_c -T_g) increases with the increase of Dy^{3+} concentration. The increase in the stability is due to the participation of Dy_2O_3 ion in the glass structure, which increases the compactness of the glass (Badamasi, 2017; Badamasi & Tanko, 2018).

Table 5 displays the values of T_g, T_c and T_m and calculated glass stability (S) and Hruby parameter for the zinc tellurite glasses. Thus, it can be inferred that since the values of ΔT_s (Table 5) are higher than 100 °*C* for all the prepared samples show that the prepared glasses have quite noble thermal stability. The growing thermal stability shows the declining crystallization tendency as demonstrated in sample with 2.5 mol% Dy^{3+} ion concentration. Hruby's parameter (*H*) evaluates glass forming ability. As can be seen in Table 4.5, changing in the Hruby's parameter with changing Dy^{3+} concentration (Badamasi & Tanko, 2018).

Table 5:Dy_2O_3 concentration dependent thermal properties of the prepared glasses.

Glass code	T_g(°*C*)	T_c (°*C*)	T_m(°*C*)	S = T_c - T_g (°*C*)	H
TZND0.0	296	406	668	110	0.4198
TZND0.4	303	427	666	124	0.5188
TZND0.8	305	459	665	154	0.7476
TZND1.2	311	436	665	125	0.5459
TZND1.6	310	438	665	128	0.5639
TZND2.5	310	439	665	129	0.5708

CONCLUSIONS

The effects of Dy^{3+} ion concentration on the absorption and the luminescence features of zinc sodium tellurite glasses are demonstrated. Thermally stable and optically transparent glass samples were prepared using melt quenching method. The physical and optical properties of the proposed glass system are found to be strongly sensitive to the Dy^{3+} contents variation. Room temperature absorption spectra exhibited seven absorption bands. The luminescence spectra revealed three significant emissions peaks with intensity enhancement. FTIR spectra of the prepared glasses revealed several bonding vibration modes in the wavenumber range of 448-468 cm^{-1}, 560-615 cm^{-1}, 772-817 cm^{-1}, 1625-1661 cm^{-1}, 2925-2944 cm^{-1} and 3445-3482 cm^{-1}. The achieved improvement in the optical properties of Dy^{3+} ions doped zinc sodium tellurite glass suggests that the proposed material composition is good for lasing purpose.

ACKNOWLEDGMENTS

The authors gratefully acknowledge the financial support provided by Ministry of Higher Education and Universiti Teknologi Malaysia through research grant of Vote number (4F424, FRGS) and (12H42 and 13H50, GUP). Also, Badamasi is grateful to Kaduna State Government, Federal Republic of Nigeria for the Study Sponsorship and National Board for Technology Incubation (N.B.T.I)/Technology Incubation Centre (T.I.C) Kano, Nigeria.

REFERENCES

Abdul Azeem, P., Balaji, S., & Reddy, R. R. (2008). Spectroscopic Properties of Dy^{3+} in NaF-B_2O_3-Al_2O_3 Glasses. *Spectrochimica Acta Part A: Molecular and Biomolecular Spectroscop, 69*, 183-188.

Agarwal, A., Pal, I., Sanghi, S., & Aggarwal, M. P. (2009). Judd-Ofelt Parameters and Radiative Properties of Sm^{3+} Ions Doped Zinc Bismuth Borate Glasses. *Optical Materials, 32*(2), 339-344.

Babu, P., Jang, K. H., Kim, E. S., Shi, L., Vijaya, R., Lavin, V., . . . Seo, H. J. (2010). Optical Properties and Energy Transfer of Dy^{3+}-Doped Transparent Oxyfluoride Glasses and Glass-Ceramics. *Journal of Non-Crystalline Solids, 356*(4), 236-243.

Badamasi, S. (2017). *Synthesis and Characterizations of Dysprosium Doped Zinc-Sodium-Tellurite Glass.* Universiti Teknologi Malaysia, Department of Physics. Johor Bahru, Johor, Malaysia: Universiti Teknologi Malaysia.

Badamasi, S., & Tanko, Y. A. (2018). Thermal Properties of TeO_2-ZnO-Na_2O Glasses: Effect of Dy_2O_3 Doping. *Science World Journal, 13*(4), 95-99.

Damak, K., El Sayed, Y., Russel, C., & Maalej, R. (2014). White Light Generation from Dy^{3+} Doped Tellurite Glass. *Journal of Quantitative Spectroscopy and Radiative Transfer, 134*, 55-63.

El-Mallawany, R. A. (2002). *Tellurite Glasses Handbook: Physical Properties and Data.* CRC Press.

El-Zaidia, M. M., Ammar, A. A., & El-Mallawany, R. A. (1985). Infra-Red Spectra, Electron Spin Resonance Spectra, and Density of $(TeO_2)100\text{-}x(WO_3)x$ and $(TeO_2)100\text{-}x\text{-}(ZnCl_2)x$ Glasses. *Physica Status Solidi (a), 91*, 637-642.

Gowda, V. V., Reddy, C. N., Radha, K. C., Anavekar, R. V., Etourneau, J., & Rao, K. J. (2007). Structural Investigations of Sodium Diborate Glasses Containing PbO, Bi_2O_3 and TeO_2: Elastic Property Measurements and Spectroscopic Studies. *Journal of Non-Crystalline Solids, 353*, 1150-1163.

Kesavulu, C. R., & Jayasankar, C. K. (2011). White Light Emission in Dy^{3+} -Doped Lead Fluorophosphate Glasses. *Materials Chemistry and Physics, 130*, 1078-1085.

Krishnaiah, K. V., Kumar, K. U., & Jayasankar, C. K. (2013). Spectroscopic Properties of Dy^{3+} -Doped Oxyfluoride glasses for White Light Emitting Diodes. *Materials Express, 3*, 61-70.

Kumar, G. A., De La Rosa, E., & Desirena, H. (2006). Radiative and Nonradiative Spectroscopic Properties of Er^{3+} Ion in Tellurite Glass. *Optics Communications, 260*(1), 601-606.

Kumar, V. M., Jamalaiah, B. C., Gopal, K. R., & Reddy, R. R. (2012). Optical Absorption and Fluorescence Studies of Dy^{3+} Doped Lead Telluroborate Glasses. *Journal of Luminescences, 132*, 86-90.

Lakshminarayana, G., & Buddhudu, S. (2006). Spectral Analysis of Sm^{3+} and Dy^{3+}:B_2O_3-ZnO-PbO Glasses. *Physica B: Condenesd Matter, 373*, 100-106.

Linganna, K., Rao, C. S., & Jayasankar, C. S. (2013). Optical Properties and Generation of White Light in Dy^{3+} -Doped Lead Phosphate Glasses. *Journal of Quantitative Spectroscopy and Radiative Transfer, 118*, 40-48.

Madhukar Reddy, C., Dillip, G. R., & Deva Prasad Raju, B. (2011). Spectroscopic and Luminescent of Dy^{3+} ions in Lead Containing Sodium Fluoroborate Glasses for Laser Materials. *Journal of Physics and Chemistry Solids, 72*, 1436-1441.

Maheshvaran, K., & Marimuthu, K. (2011). Structural and Optical Investigations on Dy^{3+} Doped Borotellurite Glasses. *Journal of Alloys and Compounds, 509*, 7427-7433.

Maheshvaran, K., Arunkumar, S., Sudarsan, V., Natarajan, V., & Marimuthu, K. (2013). Structural and Luminescence Studies on Er^{3+}/Yb^{3+} Co-doped Boro-Tellurite Glasses. *Journal of Alloys and Compounds, 56*, 142-152.

Pisarska, J. (2009). Optical Properties of Lead Borate Glasses Containing Dy^{3+} ions. *Journal of Physics Condens Matter, 21*, 285101.

Pisarska, J., Pisarska, W. A., & Ryba-Romanowski. (2010). Laser Spectroscopy of Nd^{3+} and Dy^{3+} ions in Lead Borate Glasses. *Optics & Laser Technology, 42*, 805-809.

Pisarski, W. A., Pisarski, J., Lisiecki, R., Dominiak-Dzik, G., & Ryba-Romanowski, W. (2012). Luminescence Quenching of Dy^{3+} ions in Lead Bismuthate Glasses. *Chemical Physics Letters, 531*, 114-118.

Praveena, R., R., V., & Jayasankar, C. K. (2008). Photoluminescence and Energy Transfer Studies of Dy^{3+} -Doped Fluorophosphate Glasses. *Spectrochimica Act Part A: Molecular and Biomolecular Spectroscopy, 70*, 577-586.

Rada, S., Dehelean, A., & Culea, E. (2011). FTIR and UV-VIS Spectroscopy Investigations on The Structure of the Europium-Lead-Tellurite Glasses. *Journal of Non-Crystalline Solids, 357*, 3070-3073.

Reddy, M. C., Rao, B. A., Brik, M. G., Reddy, A. P., Rao, P. R., Jayasankar, C. K., & Veeraiah, N. (2012). Emission Properties of Dy^{3+} ions in Lead Antimony Borate Glasses. *Applied Physics B, 108*, 455-461.

Saleem, S. A., Jamalaiah, B. C., Jayasimhadri, M., Rao, A. S., Jang, K., & Moorthy, L. R. (2011). Luminescent Studies of Dy^{3+} ion in Alkali Lead Tellurofluoroborate Glasses. *Journal of Quantitative Spectroscopy and Radiative Transfer, 112*, 78-84.

Sreedhar, V. B., Ramachari, D., & Jayasankar, C. K. (2013). Optical Properties of Zincfluorophosphate Glasses Doped with Dy^{3+} ions. *Physica B: Condensed Matter, 408*, 158-163.

Tanko, Y. A., Sahar, M. R., & Ghoshal, S. K. (2016). Samarium Activated Absorption and Emission of Zinc Tellurite Glass. *Jurnal Teknologi, 78*, 149-152.

Thomas, P. A. (1988). The Crystal Structure and Absolute Optical Chirality of Paratellurite, α-TeO_2. *Journal of Physics C: Solid State Physics, 21*(25), 4611.

Wang, J., Vogel, E., & Snitzer, E. (1994). Tellurite Glass: A New Candidate for Fiber Devices. *Optical Materials, 3*(3), 187-203.

Yamusa, Y. A., Hussin, R., Shamsuri, W. W., Tanko, Y. A., & Jupri, S. A. (2018). Impact of Eu^{3+} on The Luminescent, Physical and Optical Properties of $BaSO_4$-B_2O_3-P_2O_5 Glasses. *Optik, 164*, 324-334.

Zarifah, N. A., Halimah, M. K., Hashim, M., Azmi, B. Z., & Daud, W. M. (2010). Magnetic Bahaviour of $(Fe_2O_3)x$ $(TeO_2)1-x$ Glass System Due to Iron Oxide. *Chalcogenide Letters, 7*, 565-571.